An iterative Goldstein SAR interferogram filter

Article *in* International Journal of Remote Sensing · June 2012

DOI: 10.1080/01431161.2010.532171

CITATIONS
22

READS
525

4 authors, including:

Chaoying Zhao
Chang'an University
122 PUBLICATIONS **2,223** CITATIONS
SEE PROFILE

Xiaoli Ding
The Hong Kong Polytechnic University
343 PUBLICATIONS **7,251** CITATIONS
SEE PROFILE

Jing Zhang
Chang'an University
13 PUBLICATIONS **247** CITATIONS
SEE PROFILE

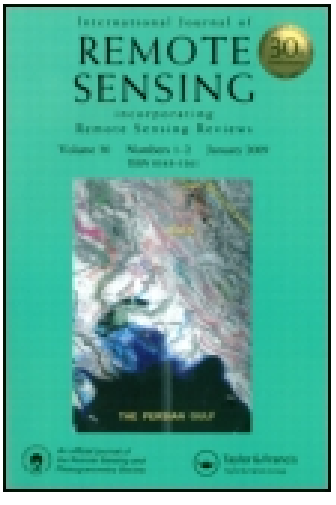

International Journal of Remote Sensing

Publication details, including instructions for authors and subscription information:
http://www.tandfonline.com/loi/tres20

An iterative Goldstein SAR interferogram filter

Chaoying Zhao [a b], Qin Zhang [a b], Xiaoli Ding [c] & Jing Zhang [a]

[a] College of Geology, Engineering and Geomatics, Chang'an University, Xian, China

[b] Key Laboratory of Western China's Mineral Resources and Geological Engineering, Ministry of Education, Xian, China

[c] Department of Land Surveying and Geo-Informatics, Hong Kong Polytechnic University, Hung Hom, Hong Kong

Published online: 24 Nov 2011.

To cite this article: Chaoying Zhao, Qin Zhang, Xiaoli Ding & Jing Zhang (2012) An iterative Goldstein SAR interferogram filter, International Journal of Remote Sensing, 33:11, 3443-3455, DOI: 10.1080/01431161.2010.532171

To link to this article: http://dx.doi.org/10.1080/01431161.2010.532171

International Journal of Remote Sensing
Vol. 33, No. 11, 10 June 2012, 3443–3455

Taylor & Francis
Taylor & Francis Group

An iterative Goldstein SAR interferogram filter

CHAOYING ZHAO*†‡, QIN ZHANG†‡, XIAOLI DING§ and JING ZHANG†
†College of Geology, Engineering and Geomatics, Chang'an University, Xian, China
‡Key Laboratory of Western China's Mineral Resources and Geological Engineering, Ministry of Education, Xian, China
§Department of Land Surveying and Geo-Informatics, Hong Kong Polytechnic University, Hung Hom, Hong Kong

(*Received 24 July 2009; in final form 13 October 2010*)

This article presents a new modified Goldstein synthetic aperture radar (SAR) interferogram filter algorithm, named the iterative Goldstein filter. The main idea of this approach is to iteratively filter the SAR interferogram, by determining the filtering parameter alpha adaptively with respect to the pseudo-correlation value of the original and/or last filtered interferograms several times. The filter can be stopped automatically by pre-setting the threshold of mean value and the improvement of pseudo-correlation in given filter windows. Experimental results with both a simulated digital elevation model (DEM) interferogram and real SAR deformation interferogram show an improvement in the new algorithm results compared with those using the Goldstein filter, and its enhanced version, the Baran filter. In addition, from a pseudo-correlation map of the iteratively filtered interferogram, some valuable information can also be abstracted based on the signal residues.

1. Introduction

Although synthetic aperture radar interferometry (InSAR) has been widely applied to measure surface topography and deformation in the last two decades (Zebker and Goldstein 1986, Massonnet and Feigl 1998), an improvement of the interferometry technique and the quality of its products is desirable to further enhance its capabilities. The accuracy of InSAR measurements is highly dependent on the quality of the interferogram formed, based on two or more synthetic aperture radar (SAR) images. Due to the effects of various decorrelation factors, such as thermal, temporal, geometrical, Doppler centroid and data processing (Zebker and Villasenor 1992), the phases of the SAR interferogram are often noisy, which can decrease the accuracy of the digital elevation model (DEM) and deformation measurement.

Unlike applications such as monitoring of earthquakes and land subsidence, where, for example, a complex multilook operation with four looks in the range direction and 20 looks in the azimuth direction was applied (Berardino *et al.* 2002), in monitoring for mine collapse or ground fissure deformation, the high spatial resolution of InSAR should be kept for great subsidence gradient monitoring, so filtering is a key step for improving the quality of the interferogram. Generally, interferogram filtering can be

*Corresponding author. Email: zhaochaoying@163.com

International Journal of Remote Sensing
ISSN 0143-1161 print/ISSN 1366-5901 online © 2012 Taylor & Francis
http://www.tandf.co.uk/journals
http://dx.doi.org/10.1080/01431161.2010.532171

divided into two main classes: filtering in the spatial and the frequency domains. So-called Lee filtering (Lee *et al.* 1998) belongs to the spatial domain filtering class, while the filtering algorithm originally proposed by Goldstein and Werner (1998), and its modified versions by Baran *et al.* (2003) and Li *et al.* (2008), belong to the frequency domain filtering methods. Based on the Goldstein filter, this article proposes another modified version, an iterative filtering algorithm, by determining the filtering parameter alpha according to the pseudo-correlation value of the original and/or last filtered interferograms.

2. Review of filtering methods in the frequency domain

2.1 *Goldstein filtering*

Goldstein and Werner (1998) proposed an adaptive radar interferogram filter based on the Fourier spectrum $Z(u, v)$ of a small interferogram patch by its smoothed absolute value $S\{Z(u, v)\}$ to the power of an exponent α, as shown as equation (1):

$$H(u, v) = S\{|Z(u, v)|\}^{\alpha}\ Z(u, v), \tag{1}$$

where $H(u, v)$ is the filter response (the spectrum of the filtered interferogram), $S\{\cdot\}$ is a smoothing operator, u, v are spatial frequencies, and α is the filtering parameter. Patches are defined as a small part of the interferogram and are overlapped to prevent discontinuities at the boundaries. The filter parameter α takes an *a priori* value between zero and one, and has the greatest impact on the filter performance. For the value of $\alpha = 0$, the multiplication factor becomes one, and no filtering occurs. However, for large values of α, the filtering is significant. So a problem occurs when a high value of parameter α is chosen, as Goldstein and Werner (1998) demonstrated: the loss of resolution in the filtered phase. On the other hand, if a small value of parameter α is applied, the filtered phases are still noisy. Therefore, there are several considerations in determining a reasonable value for the parameter α.

2.2 *Improved parameter determination for the Goldstein filter*

As the noise level can be very different in different parts of an interferogram, and the coherence is always used to estimate the quality of an interferogram, Baran *et al.* (2003) modified the filter parameter α as shown in equation (2):

$$\alpha = 1 - \bar{\gamma}, \tag{2}$$

where $\bar{\gamma}$ denotes the mean coherence value over the effective patch (patch area minus the overlap area) of an interferogram. In practice, the complex coherence γ between two complex SAR images ω_{m} and ω_{s} (the interferometric pair) can be calculated with equation (3):

$$\gamma = \frac{\sum_{i=1}^{N} \omega_{\mathrm{m}}^{i} \omega_{\mathrm{s}}^{i^*}}{\sqrt{\sum_{i=1}^{N} |\omega_{\mathrm{m}}^{i} \omega_{\mathrm{m}}^{i^*}| \sum_{i=1}^{N} |\omega_{\mathrm{s}}^{i} \omega_{\mathrm{s}}^{i^*}|}}, \tag{3}$$

where * denotes the complex conjunction, N is the number of pixels in the estimated window and i stands for the pixel index. Therefore the modification relates the degree of filtering to the coherence of an interferogram patch and makes the filter more

realistic and flexible for practical applications. By considering that phase noise is a function of both coherence and number of looks (Bamler and Hartl 1998), Li *et al.* (2008) proposed another filter parameter factor, determined by applying the standard deviation (SD) of phase noise.

However, both above-mentioned improved filters have their filtering parameters determined by the theoretical interferogram quality map, that is, coherence or SD. In practice, there are several drawbacks of coherence for assessing the quality of interferograms, such as biased estimation for the deformation interferogram if there are some systematic phases. Also, as pointed out by Li *et al.* (2004), when two mean values and SDs of coherences are quite similar, their coherence images can, however, be quite different. Lastly, the quality map can also be applied for other research related to specific decorrelation. Therefore, some other quality maps calculated from the interferogram itself will be discussed in the next §, which will be applied for filter parameter determination, some specific information detection and interferogram quality assessment in following §§.

3. The iterative Goldstein filter

3.1 *Review of interferogram quality maps*

Several interferogram quality maps have been analysed for the phase unwrapping improvement, such as coherence, SD, maximum phase gradient and pseudo-correlation (Ghiglia and Pritt 1998). For coherence, Zebker and Katherine (2005) pointed out that it is biased by a finite data sample size and any underlying interferometer fringe pattern. Hanssen (2001) has proposed an unbiased correlation estimation method by first eliminating the systematic phase, as shown in equation (4):

$$\gamma = \frac{\sum_{i=1}^{N} \omega_{\mathrm{m}}^{i} \omega_{\mathrm{s}}^{i*} \exp(-j\phi)}{\sqrt{\sum_{i=1}^{N} |\omega_{\mathrm{m}}^{i} \omega_{\mathrm{m}}^{i*}| \sum_{i=1}^{N} |\omega_{\mathrm{s}}^{i} \omega_{\mathrm{s}}^{i*}|}}, \tag{4}$$

where ϕ is the systematic phase for each pixel j means imaginary unit, and different phases of ϕ can stand for flattened, differential and/or residual phase correction cases. Li *et al.* (2004) proposed another quality map, absolute phase difference (APD), as shown in equation (5):

$$\mathrm{APD}(x, y) = \frac{1}{8} \sum_{l=-1}^{1} \sum_{k=-1}^{1} |\phi(x, y) - \phi(x + l,\ y + k)|, \tag{5}$$

where l and k are the integral variables and the sum of phase difference (SPD) can be applied as the quantitative measure for the whole interferogram quality, as in equation (6):

$$\mathrm{SPD} = \sum_{x=1}^{p} \sum_{y=1}^{q} (\mathrm{APD})(x, y), \tag{6}$$

Where p and q are the pixel numbers in the x and y directions respectively. This will be applied in this article for the quality assessment of interferograms.

The pseudo-correlation (P_{c}) map is calculated from the interferogram itself, defined as in equation (7):

$$P_{\mathrm{c}} = \frac{|\sum_{i=1}^{N} \phi_i|}{\sum_{i=1}^{N} |\phi_i|}, \tag{7}$$

where N is the total number of pixels in the estimated patch and ϕ_i is the interferogram value. In this article, the pseudo-correlation quality map will be taken to determine the filter factor iteratively and to detect the signal residues to show the ground discontinuous region, that is, ground fissures, in the real SAR data test §.

3.2 *The iterative Goldstein filter method*

Originally, Katsaggelos and Tsai (2005) researched the theory and method of iterative image restoration, where the restoration algorithms, convergence and constraints for solution of the amplitude image were analysed. Here, we focus only on the complex phase filtering under the framework of the Goldstein filter. Similarly, the filter parameter α is determined from the pseudo-correlation map of the interferogram to be filtered as shown in equation (8):

$$\alpha = 1 - \bar{c}, \tag{8}$$

where $\bar{c}$ is the mean value of pseudo-correlation values in the filtered windows. After the first filtering, if the interferogram is still noisy (as indicated by P_{c}), it can be filtered a second time; meanwhile, the parameter factor is calculated based on the first-filtered interferogram, which is called the iterative Goldstein filter. A flow chart of the iterative Goldstein filter is shown in figure 1 (modified from Baran 2004), where the number of filtering iterations can be automatically determined by *a priori* thresholds of the mean pseudo-correlation and the relative improvement of the mean pseudo-correlation.

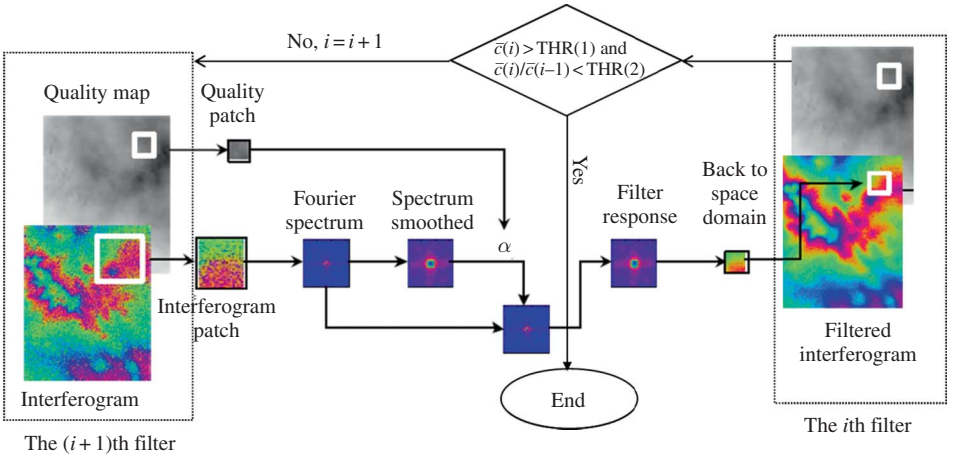

Figure 1. Flow chart of the iterative Goldstein filter, where THR stands for threshold, '$\bar{c}(i) >$ THR(1)' means the mean value of pseudo-correlation in the ith filter is larger than the first given threshold, and '$\bar{c}(i)/\bar{c}(i-1) <$ THR(2)' means the improvement of the mean value of P_{c} in the ith filter is less than the second given threshold.

4. Numerical validation using a simulated data set

The performance of the modified filter will be evaluated with simulated data sets in this section and with real data sets in the next. Comparisons with the Goldstein filter and one of the previous modifications of the Goldstein filter by Baran *et al.* (2003) will also be made. For simplicity, hereinafter, the modification proposed by Baran *et al.* (2003) and given in equation (2) will be named the Baran filter, and the new, modified filter will be referred to as the iterative filter. First a simple example is given, to show that the iterative filter can work well, and then a complex real deformation interferogram with high frequency signals is shown, to demonstrate the necessity for, and some new applications of, the iterative filter.

A multifractal DEM with a resolution of 20 m × 20 m and size 512 × 512 pixels is first simulated, based on the common values of the multifractal parameters of topography given by Pecknold *et al.* (1993). The DEM, along with the European Remote Sensing 1/2 (ERS-1/2) imaging parameter and a perpendicular baseline of 200 m, is then used to simulate 'true' interferometric phases (see figure 2(*a*)). A coherence map is also simulated, considering the thermal, geometrical and temporal decorrelation (Lee and Liu 1999), and shown in figure 3(*a*). Based on the coherence map, a phase SD map with single look numbers is then obtained. Then the interferometric phase noise is simulated based on the corresponding phase SD map and the normal noise model. Finally, the simulated observed phase (figure 2(*b*)) is generated by adding the simulated noise to the true interferometric phase values. Here, no intensity is considered. A short black line in figure 2(*a*) indicates the cross-section location.

The simulated interferogram is filtered with the Goldstein, Baran and iterative filters respectively. The patch size chosen is 32 × 32 pixels and the overlaps between patches are taken as 28 pixels to avoid discontinuities. The parameter of the Goldstein filter is 0.5 to avoid over-filtering, the parameter for the Baran filter is calculated based on equation (2) and shown as figure 3(*a*); while for the iterative filter, two filtering iterations are performed and the parameters are calculated based on equation (8). The pseudo-correlation maps of the observed and first-filtered interferograms are shown in figure 3(*b*) and (*c*), respectively. By comparing coherence and pseudo-correlation maps, some differences are clear to see. The interferograms filtered with the Goldstein and Baran filters, and second-filtered by the iterative method, are shown in figure 4.

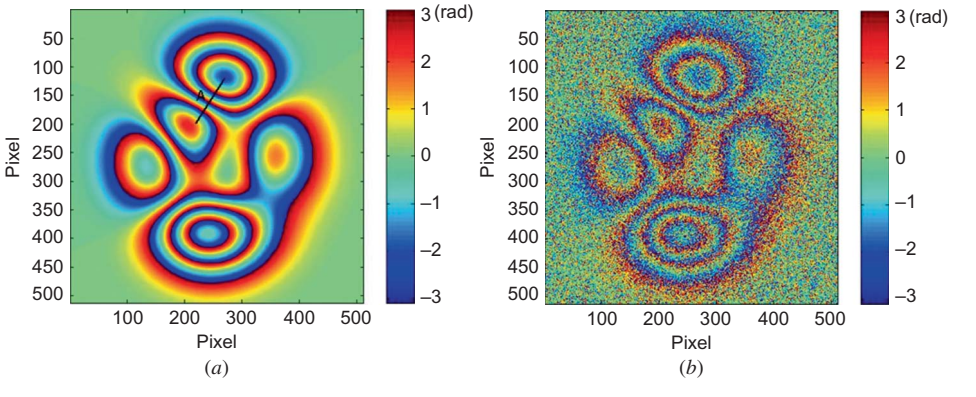

Figure 2. Simulated (*a*) true phase and (*b*) observed phase maps of one known DEM.

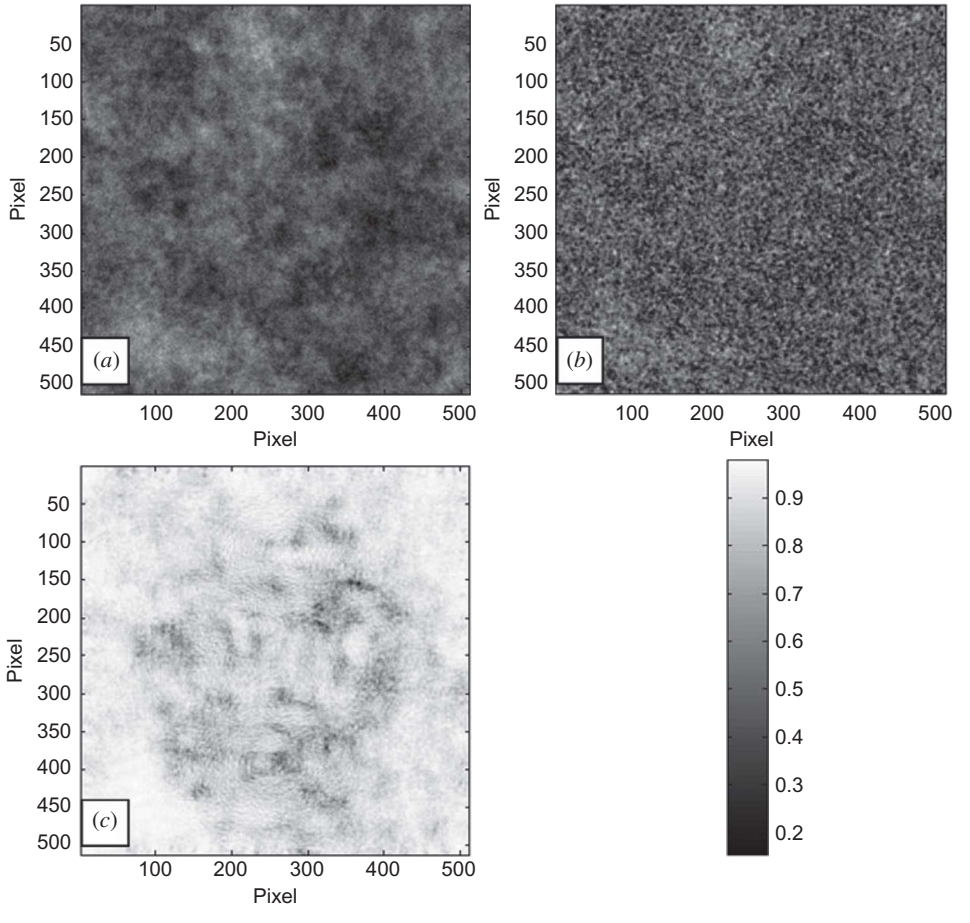

Figure 3. Quality map of simulated phase: (*a*) simulated coherence map, (*b*) pseudo-correlation map of simulated observed interferogram and (*c*) pseudo-correlation map of first-filtered interferogram. Grey colour bar indicates range from 0 to 1.

For a quantitative evaluation, the sum of phase difference and sum of residues are calculated and listed in table 1, where it can be seen that the added Gaussian noise makes the sum of phase difference (SPD) of the observed interferogram about 16 times that of the 'true' interferogram and the total number of residues increased to 63 097 from 0, which accounts for 24.1% of total pixels. The Goldstein and Baran filters can reduce the phase differences to 55% and 66% of the observed ones and reduce the phase residues to nearly one tenth and two tenths, respectively. As for the iterative filter, the first-filtered interferogram has fewer residues than those filtered by the Goldstein and Baran filters, and the second filtering can obtain a filtered interferogram with zero residues. In this simulated test, in which only noise residues are contained, thus showing the advantages of adaptive filtering in the spatial region and iterative filtering in the temporal region, the new proposed algorithm may slightly over-filter the interferogram. Under these conditions, the fewer the residues, the more reliable the unwrapping will be.

For a closer examination of the results, a cross-section, as marked on figure 2(*a*), is plotted for each of the interferograms, including the 'true', observed and filtered ones,

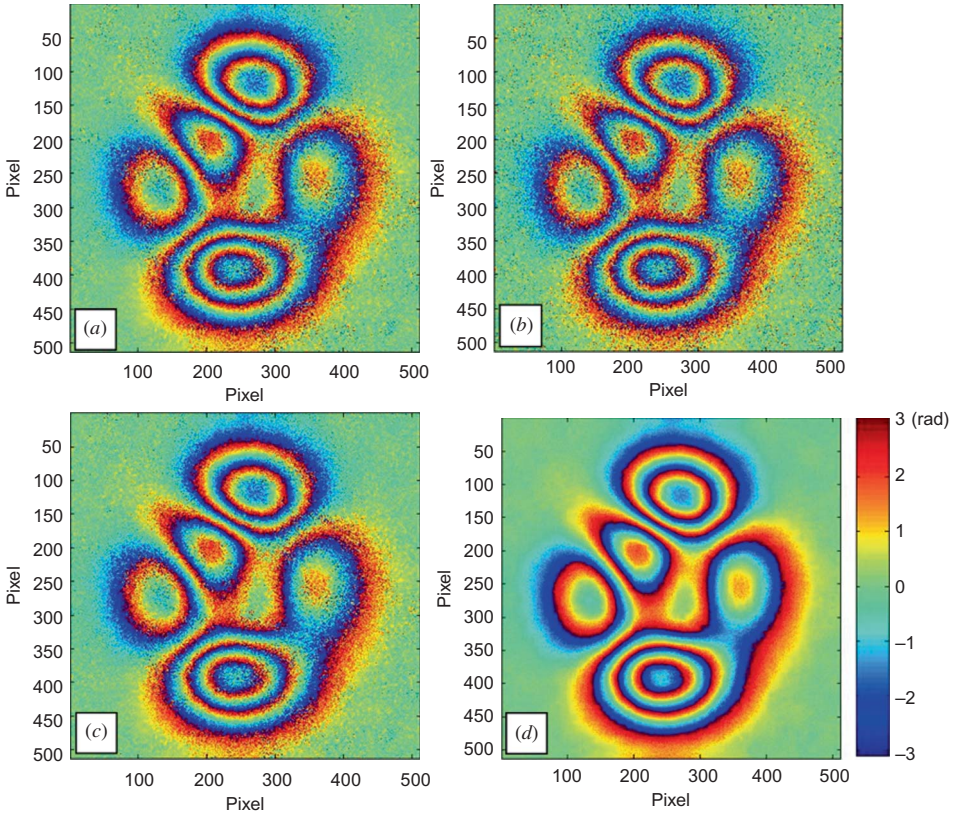

Figure 4. Filtered interferograms with different methods to simulate data: (*a*) the Goldstein filter (0.5), (*b*) the Baran filter, (*c*) first-filtered with the iterative filter and (*d*) second-filtered with the iterative filter.

Table 1. The SPD and residue proportion of the original interferogram and those after the different filters with simulated interferogram.

Interferogram	SPD × (10^5)	Residue proportion (%)
'True'	0.28389	0
Observed	4.6700	24.1
Goldstein filter	2.5617	2.5
Baran filter	3.0850	4.7
First iterative filter	2.3352	1.4
Second iterative filter	0.76395	0

and is shown in figure 5. From this figure, it is clear to see that the filtered interferometric phase values from the second iterative filter can get the closest fit with the true phase simulated. Further, it can be seen that in most regions, such as those marked 1 and 2 in figure 5, there is no improvement in the second-filtered interferogram over the first-filtered interferogram, while in some other regions, such as those marked 3 and 4 in figure 5, the improvement is significant and necessary.

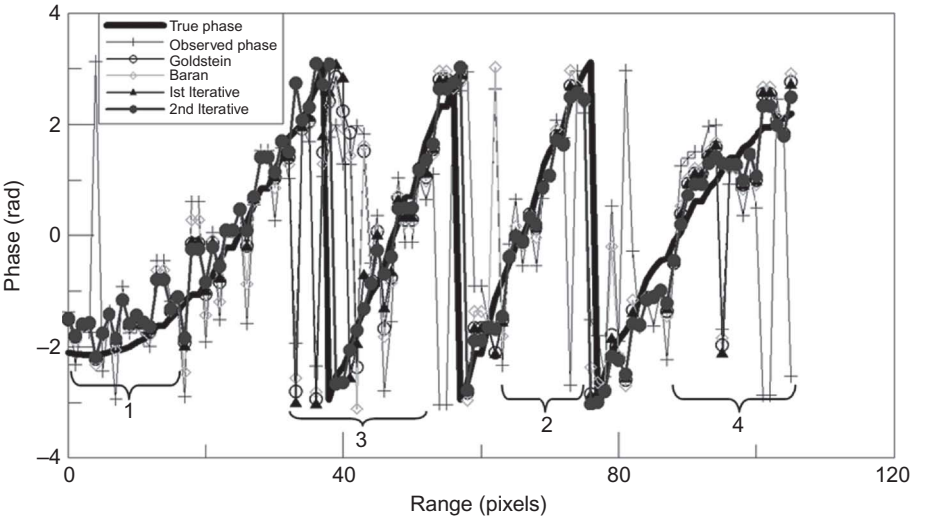

Figure 5. The cross-section of the simulated data over the unfiltered (observed) and filtered wrapped phase interferograms, filtered with the Goldstein, Baran and iterative filters.

5. Validation with real data

A real deformation pair of ERS data (frame: 2916, track: 161) acquired on 7 January and 1 July 1996 over Xian, China, which suffers from heavy signal residues caused by a large deformation gradient (generally called a ground fissure), is used to assess the performance of the iterative Goldstein filter. The perpendicular baseline of this pair is only 21 metres and the temporal baseline only 176 days, so it is feasible for differential interferometry. Under these conditions, it is supposed that the signal residues do not result from topographic effects and temporal decorrelation, but the high deformation gradient, which is larger than the InSAR monitoring limit – half a wavelength between two neighbouring pixels (Massonnet and Feigl 1998) – in a certain direction. This complex interferogram has been multilooked with one look in the range direction and five looks in the azimuth direction respectively, therefore, in total, 1500×1500 pixels in SAR coordinates will be focused on. Figure 6 shows the original differential interferogram and its coherence map; the latter will be used for the Baran filter. Again, a short black bar in figure 6(*a*) indicates the location of the cross-section. From the coherence map, the urban region in the central map is highly correlated, while the surroundings are agricultural regions, which show heavy noise. Figure 7 shows the interferograms filtered with (*a*) the Goldstein filter with $\alpha = 0.5$, (*b*) the Baran filter, and (*c*) and (*d*) the iterative filter for the first and second filters respectively.

Quantitative assessments of the iterative filter are also shown in table 2 using the sum of phase difference and residues criteria, where it can be seen that the Goldstein, Baran and first iterative filters can give similar results, but the second iterative filter can greatly improve the results. The great number of residues after the second iterative filter mainly results from the large agricultural area in this research region.

The cross-section marked on figure 6(*a*) is, as before, plotted for each of the five interferograms, and shown in figure 8. As expected, the iterative filter gives a smoother

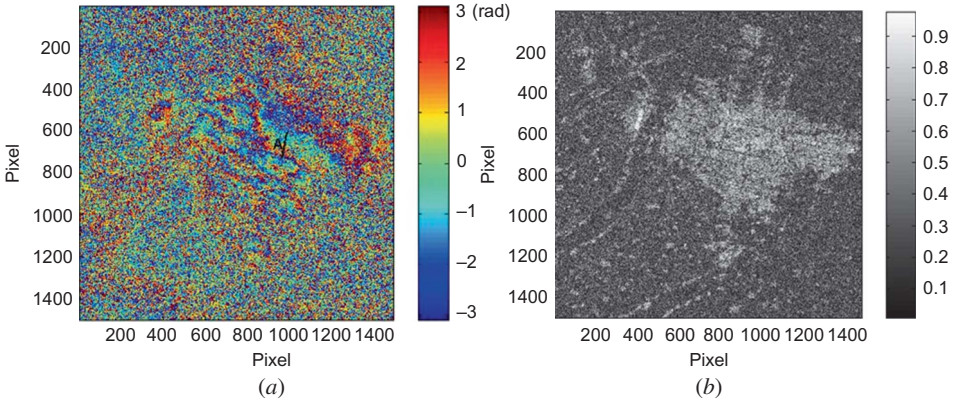

Figure 6. (*a*) The original interferogram and (*b*) its coherence map of real SAR data.

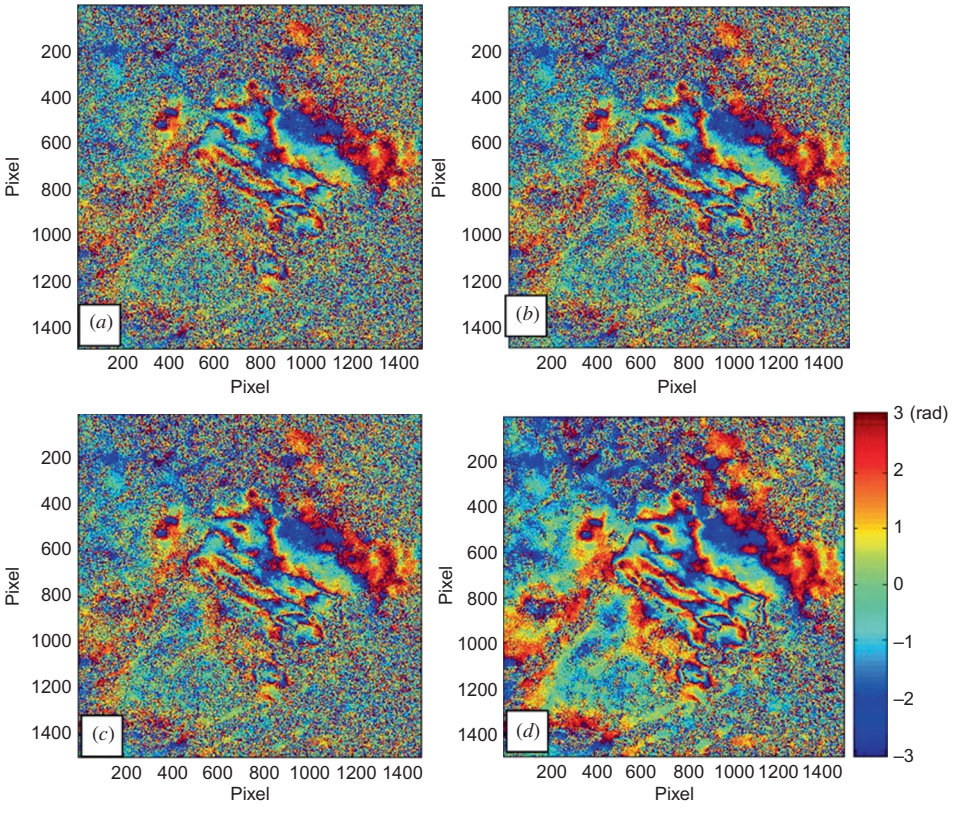

Figure 7. Interferograms filtered with different methods to the real SAR data: (*a*) the Goldstein filter (0.5), (*b*) the Baran filter, (*c*) first-filtered with the iterative filter and (*d*) second-filtered with the iterative filter.

phase than do the Goldstein and Baran filters, and the second-filtered result is better than the first-filtered one. Also, some improvement can be seen after the second filtering.

Table 2. The SPD and residue proportion of the original interferogram and those after the different filters with real SAR data.

Interferogram	SPD ($\times 10^6$)	Residue proportion (%)
Original	4.3020	24.0
Goldstein filter	3.8652	18.2
Baran filter	3.8085	16.7
First iterative filter	3.7780	16.4
Second iterative filter	2.9649	8.7

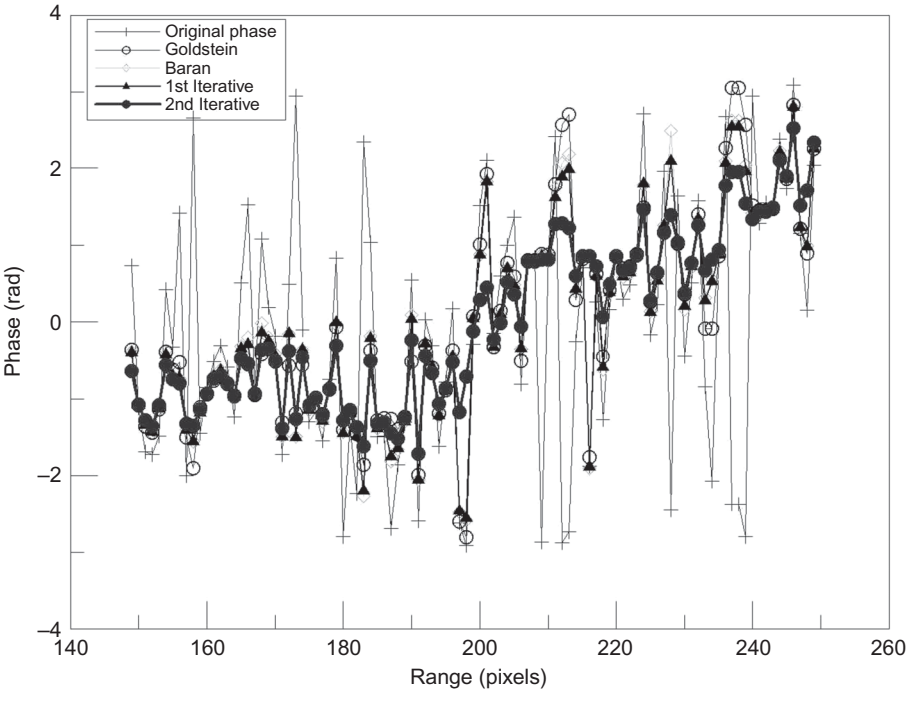

Figure 8. Cross-section of interferometric phases with the real SAR data of the observed (original) and filtered interferograms, filtered with the Goldstein, Baran and iterative filters.

In order to closely assess the newly proposed filter algorithm, nine discrete spirit levelling data recorded during a similar time span are used to validate the geocoded deformation results after the second iterative filtering (shown in figure 9) (Zhao *et al.* 2009a). The figure shows thirteen ground fissures and the spirit levelling benchmarks superimposed on the background of the intensity map. A comparison between the Baran and second-filtered deformation results is shown in table 3. As well as this, the pseudo-correlation map can also be applied to detect the location of signal residues, which are physically related to the active ground fissures in this example. To highlight the signal residues, we have generated a texture map by calculating the SD to mean value ratio for a given pixel within a 5×5 windows of the pseudo-correlation map after the second filtering, which is superimposed with known ground fissures and shown in figure 10 (Zhao *et al.* 2009b).

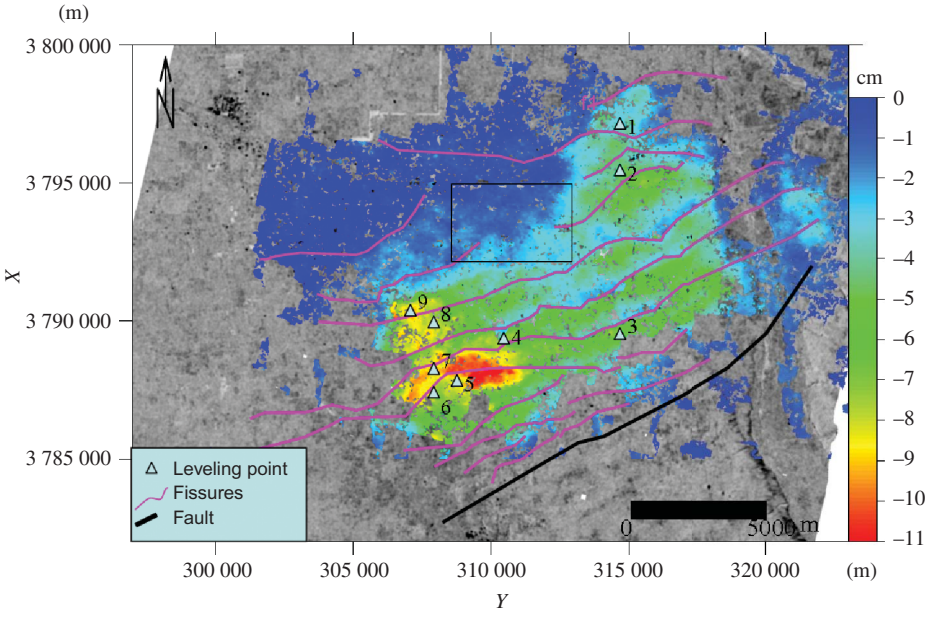

Figure 9. Geocoded deformation map between 7 January and 1 July 1996, where pink lines show the location of active ground fissures in Xian city, the nine cyan triangles are the levelling points, the dark triangle is a reference point in a stable region, the black line is an active fault in Xian and the background is the intensity map.

Table 3. Statistics of the Baran and second-filtered deformation with discrete levelling points (in cm).

No.	Levelling	Baran	Δ*	Iterative	Δ*	Location
1	−3.9	−4.5	0.6	−4.3	0.4	Xinjiamiao
2	−5.3	−6.2	0.9	−5.8	0.5	Hujiamiao
3	−4.3	−4.9	0.6	−4.8	0.5	Tielumiao
4	−7.2	−6.5	−0.7	−7.2	0.0	Xiaozhai
5	−6.8	−7.2	0.4	−7.2	0.4	Balicun
6	−7.2	−6.0	−1.2	−6.3	−0.9	Hi-tech zone
7	−5.3	−6.5	1.2	−6.3	1.0	
8	−4.8	−5.4	0.6	−5.3	0.5	
9	−6.3	−7.5	1.2	−7.2	1.1	
Standard deviation			±0.8		±0.6	

Note: *Difference between levelling result and the filtered InSAR deformation result.

The good results in comparison with the spirit-levelling data show an improvement for unwrapping and deformation monitoring; the levelling benchmarks were originally sited for land subsidence monitoring, so they are not near the ground fissure region.

Figure 10 shows that the pseudo-correlation map can also be applied for positioning or tracing large deformation gradient regions, which would be beneficial to geological research.

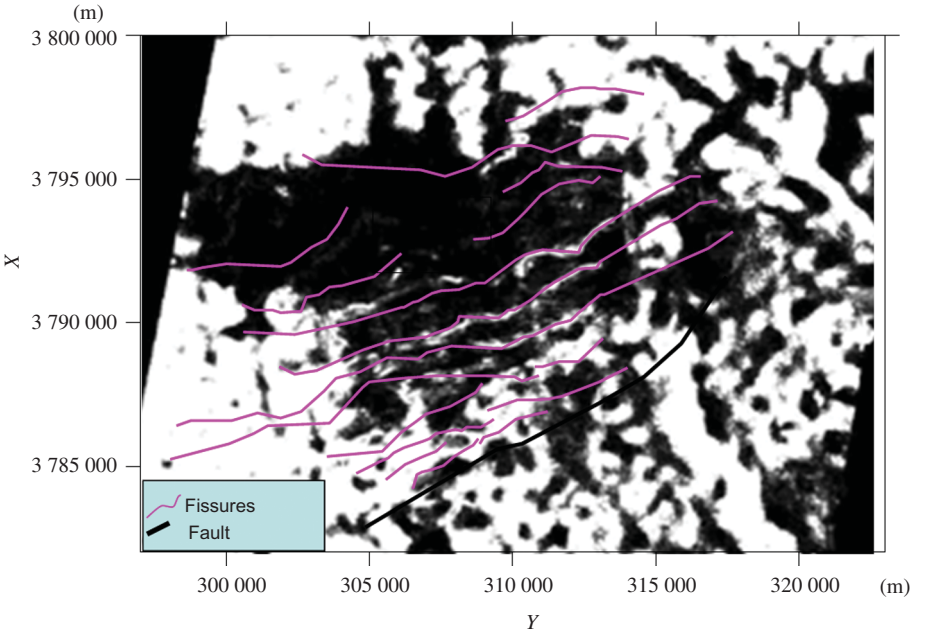

Figure 10. The overlay map of known ground fissures and detected active fissures during the monitoring time span in 1996; the background is the texture of the pseudo-correlation map after second filtering.

6. Conclusion

A new modification of the Goldstein filter is proposed, which involves iteratively filtering the interferograms, and the filter parameter is determined from the pseudo-correlation of the original and/or last-filtered interferograms. In practice, the filter parameter alpha determined from pseudo-correlation is more reasonable than that given an *a priori* value or determined by a theoretical coherence value. Results from two tests carried out with a simulated DEM phase and real deformation phase have shown the newly proposed iterative Goldstein filter can improve the interferogram quality, hence improve final results such as DEM or deformation. In addition, the pseudo-correlation map of the iteratively filtered interferogram can also abstract valuable information, such as the position of active ground fissures.

Acknowledgements

The SAR data were supplied by the European Space Agency (ESA) under category-1. This research was funded by the Natural Science Foundation of China (NSFC) (No. 40802075, 41072266) and the key project of the Ministry of Land & Resources, China (No. 1212010914015). We greatly thank the two anonymous reviewers of this manuscript for their helpful and constructive comments.

References

Bamler, R. and Hartl, P., 1998, Synthetic aperture radar interferometry. *Inverse Problems*, **14**, pp. R1–R54.

Baran, I., 2004, Advanced satellite radar interferometry for small scale surface deformation detection. PhD dissertation, Curtin University of Technology, Sydney.

Baran, I., Stewart, M.P., Kampes, B.M., Perski, Z. and Lilly, P., 2003, A modification to the Goldstein radar interferogram filter. *IEEE Transactions on Geoscience and Remote Sensing*, **41**, pp. 2114–2118.

Berardino, P., Fornaro, G., Lanari, R. and Sansosti, E., 2002, A new algorithm for surface deformation monitoring based on small baseline differential SAR interferometry. *IEEE Transactions on Geoscience and Remote Sensing*, **40**, pp. 2375–2383

Ghiglia, D.C. and Pritt, M.D., 1998, *Two-dimensional phase unwrapping: theory, algorithms, and software*, pp. 70–82 (New York, NY: John Wiley & Sons).

Goldstein, R.M. and Werner, C.L., 1998, Radar interferogram filtering for geophysical applications. *Geophysical Research Letters*, **25**, pp. 4035–4038.

Hanssen, R.F., 2001, *Radar Interferometry – Data Interpretation and Error Analysis*, 98 pp. (Dordrecht: Kluwer Academic).

Katsaggelos, A.K. and Tsai, C.J., 2005, Iterative image restoration. In *Handbook of Image and Video Processing*, A. Bovik (Ed.), pp. 235–252 (Burlington, MA: Elsevier Academic Press).

Lee, H. and Liu, J.G., 1999, Spatial decorrelation due to topography in the interferometry SAR coherence imagery. In *Proceedings of IEEE 1999 International Geoscience and Remote Sensing Symposium*, 28 June–2 July 1999, Hamburg, Germany (Burlinton, MA: Elsevier Academic Press), pp. 485–487.

Lee, J.S., Papathanassiou, K., Ainsworth, T.L., Grunes, M.R. and Reigber, A., 1998, A new technique for noise filtering of SAR interferometric phase images. *IEEE Transactions on Geoscience and Remote Sensing*, **36**, pp. 1456–1465.

Li, Z.L., Zou, W.B., Ding, X.L., Chen, Y.Q. and Liu, G.X., 2004, A quantitative measure for the quality of InSAR interferograms based on phase differences. *Photogrammetric Engineering and Remote Sensing*, **70**, pp. 1131–1137.

Li, Z.W., Ding, X.L., Huang, C., Zhu, J.J. and Chen, Y.L., 2008, Improved filtering parameter determination for the Goldstein radar interferogram. *ISPRS Journal of Photogrammetry and Remote Sensing*, **63**, pp. 621–634.

Massonnet, D. and Feigl, K.L., 1998, Radar interferometry and its application to changes in the earth's surface. *Reviews of Geophysics*, **36**, pp. 441–500.

Pecknold, S., Lovejoy, S., Schertzer, D., Hooge, C. and Malouin, J.F., 1993, The simulation of universal multifractals. In *Cellular Automata: Prospects in Astrophysical Applications*, A. Lejeune and J. Perdang (Eds.), pp. 228–267 (Singapore: World Scientific).

Zebker, H.A. and Goldstein, R.M., 1986, Topographic mapping from interferometric synthetic aperture radar observations. *Journal of Geophysical Research*, **91**, pp. 4993–4999.

Zebker, H.A. and Katherine, C., 2005, Accurate estimation of correlation in InSAR observations. *IEEE Geoscience and Remote Sensing letters*, **2**, pp. 124–127.

Zebker, H.A. and Villasenor, J., 1992, Decorrelation in interferometric radar echoes. *IEEE Transactions on Geoscience and Remote Sensing*, **30**, pp. 950–959.

Zhao, C.Y., Zhang, Q., Ding, X.L., Peng, J.B. and Yang, C.S., 2009a, InSAR based evaluation of land subsidence and ground fissure evolution at Xian. *Journal of Engineering Geology*, **17**, pp. 389–393 [in Chinese].

Zhao, C.Y., Zhang, Q., Ding, X.L. and Qu, W., 2009b, Positioning of Xian active ground fissures with SAR interferometry. *Geomatics and Information Science of Wuhan University*, **34**, pp. 809–813 [in Chinese].